Science Bulletin of National Chiao Tung University, Vol. VI, No. 1

LARGE-SIGNAL ANALYSIS OF BARITT DIODES

J. L. CHU

Chung-Shan Institute, Chung-Li, Taiwan, China

and

S. M. SZE

College of Engineering, National Chiao Tung University and
Bell Telephone Laboratories, Murray Hill, New Jersey, U. S. A.

(Received November 24, 1972)

Abstract—*Large-Signal properties of $p^+\nu np$ and associated BARITT (Barrier Injection Transit Time) diodes are analyzed. An accurate computer program (Sempak) is used which considers the space-charge balance, dependence of carrier mobilities on impurity concentration and electric field, and carrier generation and recombination.*

The static properties of BARITT diodes are also considered. General expressions for the flat-band voltage and the differential reactance are obtained. The results show that the $p^+\nu np$ structure is the best choice which gives optimum performances both in static and microwave characteristics.

I. INTRODUCTION

We use an accurate computer program-LL, AID, M1557, for describing the dynamics of holes, electrons and electric field profiles in one-dimensional semiconductor structures. The physical phenomena considered are: drift and diffusion of charged carriers, space charge balance (Poisson's equation), dependence of carrier mobilities (diffusion) on impurity concentration and electric field strength, carrier generation and recombination by Shockley-Read-Hall centers, and implicitly the temperature effect. The computed results for simply p^+np^+ and $p^+\nu np$ BARITT diodes are shown in Fig. 1 and Fig. 9.

From the static and microwave performance of the simple p^+np^+ diode, we obtain (1) under relatively large current density such as 30 A/cm², the electric field in most part of the drift region is lower than the critical field E_s (Fig. 1), and the injected carriers will drift through low fields at the beginning of the journey, which causes the device to operate at low frequencies than the transit-time frequency; (2) Since at the field region, the velocity of the drift carriers is a function of the field so that if there are any fluctuations of bias current, the drift velocity of carrier will be changed, and the output power as well as the operation frequency will be unstable, and (3) from the microwave measurement (Figure 2), it shows that the microwave output power and efficiency are functions of *dc* bias

currents. If we compare the *dc* current at maximum efficiency point with the *dc* current-voltage curves (Figure 3), we note that the corresponding current is at the point where it is influenced by the space-charge-limited effect and starts to bend. Thus the space-charge-limited effect causes the efficiency of the doide to decrease.

Hence for efficient microwave operation of a BARITT diode, it is desirable to have (1) a uniform electric field in the drift region sufficient to cause the carriers to drift at their scattering-limited velocity over the entire drift region, (2) a low operation voltage to eliminate the need of high-voltage supply, and (3) opposite dopings in the injection and drift region so that the space-charge-effect can be reduced or eliminated.

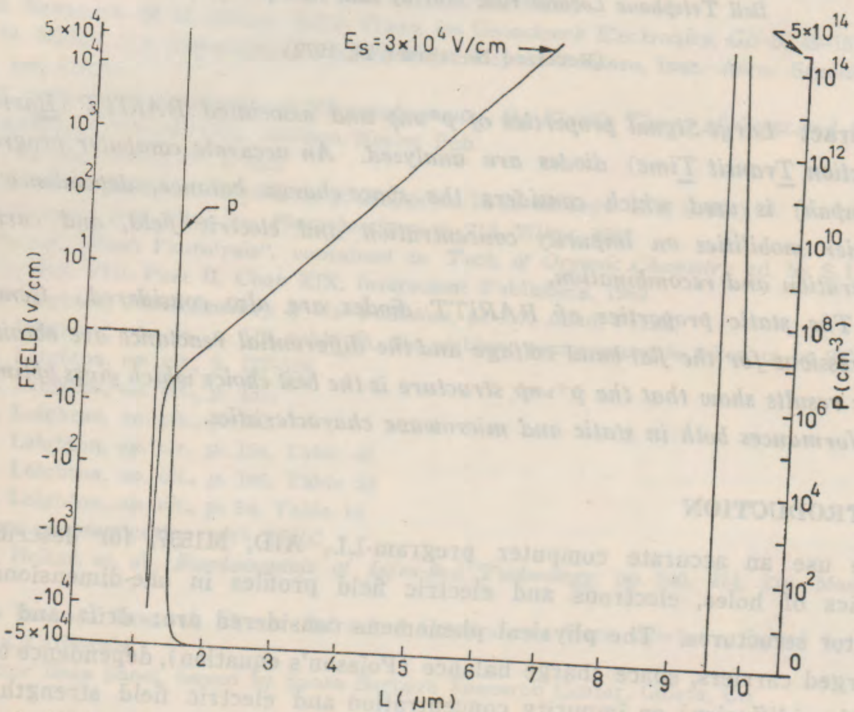

Fig. 1. Field and doping profile of p^+np^+ diode under 0.1 A/cm² current bias. The device parameters are: L=8.5 μm, $N_D = 5\times10^{14}$ cm^{-3}.

Apparently the initial p^+np^+ (or MSM) structure cannot fulfill the above requirements. We have considered various structures and concluded that the $p^+\nu np$ structure and its complimentary $n^+\pi pn$ (or Mνnp or Mπpn) structures are the best choise which can meet the above requirements (where M stands for metal, ν and π for low-doping *n*-type and *p*-type semiconductors, and *n* and *p* are for *n*-type and *p*-type semiconductors respectively).

One of the most important device design parameters for a BARITT diode is the flat-band voltage. This voltage is closely related to the operating bias voltage for high injection current and is defined as the asymptotic voltage at which the energy band at the forward-biased contact becomes flat. We shall first devive that flat-band voltage for $p^+\nu np$ structure in secotion II.

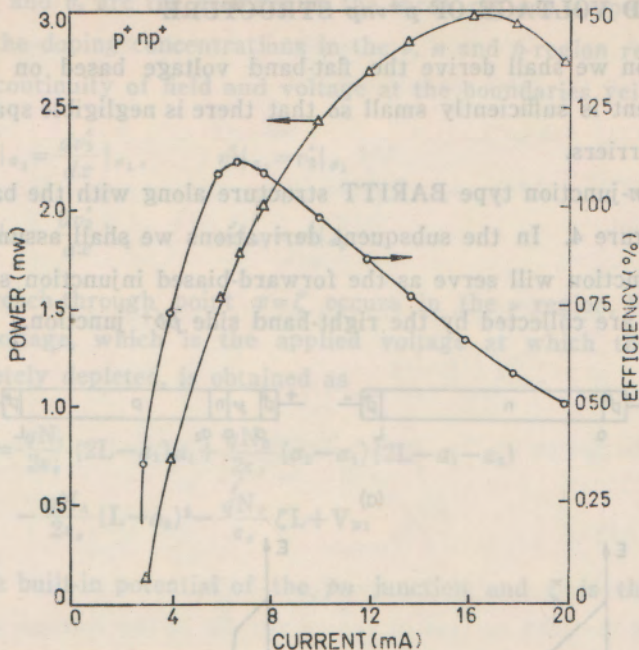

Fig. 2. Measured output power and efficency as function of bias current for the same p^+np^+ diode as in Fig. 1.

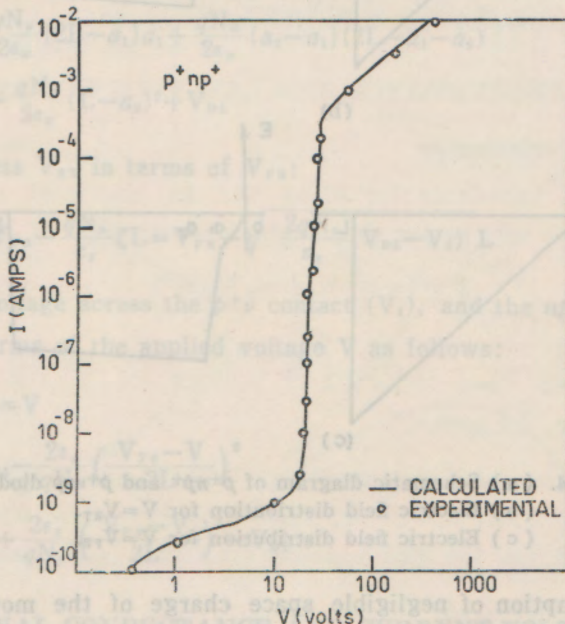

Fig. 3. Theoretical and measured I–V curve of the same p^+np^+ diode as above.

Another important design parameter is the differential conductance which characterizes the increametal increase of current with bias voltage. We shall consider the differential conductance and I–V characteristics of the $p^+\nu np$ structure in section III. The microwave perfermance and the large signal analysis are presented as section IV. A discussion is given in section V.

II. FLAT BAND VOLTAGE OF $p^+\nu np$ STRUCTURE

In this section we shall derive the flat-band voltage based on the assumption that the *dc* current is sufficiently small so that there is negligible space-charge effect due to mobile carriers.

The $p^+\nu np$ *pn*-junction type BARITT structure along with the basic p^+np^+ diode are shown in Figure 4. In the subsquent derivations we shall assume that the left-hand side $p^+\nu$ junction will serve as the forward-biased injunction source while the injected carriers are collected by the right-hand side pp^+ junction.

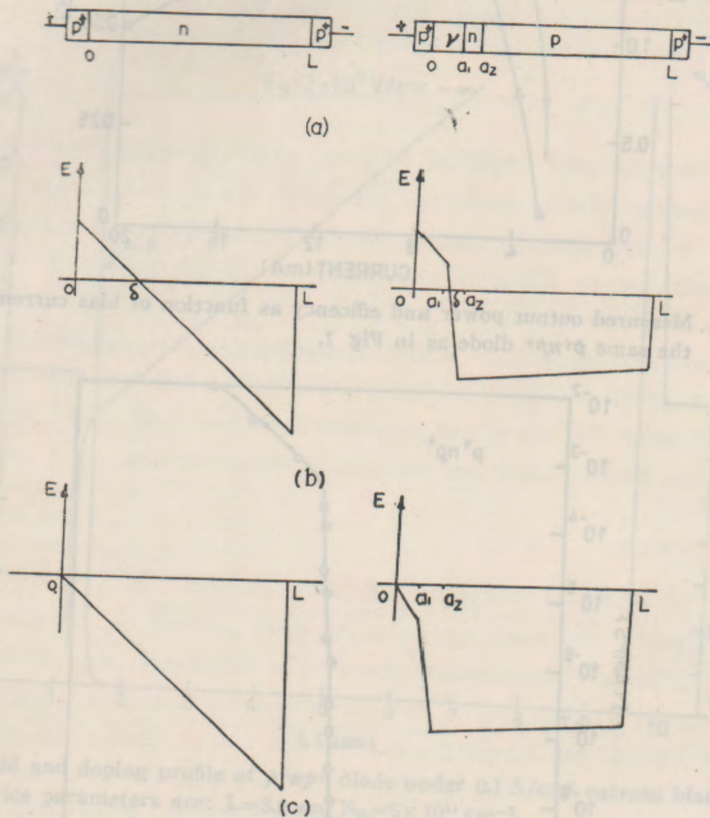

Fig. 4. (a) Schematic diagram of p^+np^+ and $p^+\nu np$ diodes.
(b) Electric field distribution for $V=V_{RT}$.
(c) Electric field distribution for $V=V_{FB}$.

Under the assumption of negligible space charge of the moving carriers, the Poissin equations for the three regions are:

$$\frac{d^2v_1'}{dx^2}=-\frac{qN_\nu}{\varepsilon_s} \qquad (0<x<a_1) \tag{1}$$

$$\frac{d^2v_2'}{dx^2}=-\frac{qN_D}{\varepsilon_s} \qquad (a_1<x<a_2) \tag{2}$$

$$\frac{d^2v_3'}{dx^2}=+\frac{qN_A}{\varepsilon_s} \qquad (a_2<x<L) \tag{3}$$

Where v_1', v_2' and v_3' are the voltages in the three regions respectively, and N_ν, N_D and N_A are the doping concentrations in the ν, n and p-region respectively. The requirement of continuity of field and voltage at the boundaries yeilds:

$$\frac{dv_1'}{dx}\Big|_{a_1}=\frac{dv_2'}{dx}\Big|_{a_1}, \qquad v_1'|_{a_1}=v_2'|_{a_1} \tag{4}$$

$$\frac{dv_2'}{dx}\Big|_{a_2}=\frac{dv_3'}{dx}\Big|_{a_2}, \qquad v_2'|_{a_2}=v_3'|_{a_2} \tag{5}$$

When the reach-through point $x=\zeta$ occurs in the ν region, Figure 4 (b), the reach-through voltage, which is the applied voltage at which the semiconductor region is completely depleted, is obtained as

$$V_{RT}=\frac{qN_1}{2\varepsilon_s}(2L-a_1)a_1+\frac{qN_D}{2\varepsilon_s}(a_2-a_1)(2L-a_1-a_2) -\frac{qN_A}{2\varepsilon_s}(L-a_2)^2-\frac{qN_\nu}{\varepsilon_s}\zeta L+V_{D1} \tag{6}$$

where V_{D1} is the built-in potential of the pn junction and ζ is the reach-through point.

It is obvious that under flat-band condition, Figure 4 (c), ζ becomes zero. We obtain from Eq. (6) the flat-band voltage

$$V_{FB}=\frac{qN_\nu}{2\varepsilon_s}(2L-a_1)a_1+\frac{qN_D}{2\varepsilon_s}(a_2-a_1)(2L-a_1-a_2) -\frac{qN_A}{2\varepsilon_s}(L-a_2)^2+V_{D1} \tag{7}$$

We can also express V_{RT} in terms of V_{FB}:

$$V_{RT}=V_{FB}-\frac{qN_\nu}{\varepsilon_s}\zeta L=V_{FB}-\sqrt{\frac{2qN_\nu}{\varepsilon_s}(V_{D1}-V_1)}\,L \tag{8}$$

For $V>V_{RT}$, the voltage across the $p^+\nu$ contact (V_1), and the np junction (V_2), can be expressed in terms of the applied voltage V as follows:

$$V_1+V_2=V \tag{9}$$

$$V_1=V_{D1}-\frac{2\varepsilon_s}{qN_\nu}\left(\frac{V_{FB}-V}{2L}\right)^2 \tag{10}$$

$$V_2=V+\frac{2\varepsilon_s}{qN_\nu}\left(\frac{V_{FB}-V}{2L}\right)^2-V_{D1} \tag{11}$$

III. DIFFERENTIAL CONDUCTANCE AND CURRENT-VOLTAGE CHARACTERISTICS OF $p^+\nu np$ STRUCTURE

When the applied voltage is smaller than the reach-through voltage, the total current is very small. This is because of the reverse-biased np junction, and the current in this region is determined by the leakage current. In the following studies we shall concentrate on the current-voltage characteristics for applied voltage equal or larger than the reach-through voltage V_{RT}.

1. For $V=V_{RT}$

Following the same approach as outlined for the Metal-semiconductor-Metal structure[1] we obtain the total current density

$$J=A^*T^2e^{-\beta V_{D1}}(e^{\beta V_1}-1) \tag{12}$$

Where $\beta\equiv q/kT$ and A^* is the effective Richardson constant for the pn junction BARITT structure[2].

2. For $V_{RT}<V<V_{FB}$

From Eqs. (10) and (12) we obtain the total current density

$$J=A^*T^2[e^{-\beta\frac{2\varepsilon_s}{qN_\nu}\left(\frac{V_{FB}-V}{2L}\right)^2}-e^{-\beta V_{D1}}] \tag{13}$$

At $V=V_{FB}$, the factor in the square brackets approaches unity and the total current becomes

$$J_{FB}=A^*T^2 \tag{14}$$

3. Differential Conductance (dJ/dv) for $V_{RT}<V<V_{FB}$

It is apparent that the current increases rapidly in the voltage range $V_{RT}<V<V_{FB}$. The differential conductance in this region can be obtained from Eq. (13)

$$\left.\frac{dJ}{dV}\right|_{V_{RT}<V<V_{FB}}=\frac{\beta\varepsilon_s}{qN_\nu L^2}[J_{FB}(V_{FB}-V)]e^{-\beta\frac{2\varepsilon_s}{qN_\nu}\left(\frac{V_{FB}-V}{2L}\right)^2} \tag{15}$$

IV. MICROWAVE PERFERMANCE AND LARGE SIGNAL ANALYSIS

1. Microwave Perfermance

The small-signal impedance for $p^+\nu np$ and its associated structures can be expressed in the same way as for simple p^+np^+ structure[3].

$$\begin{aligned}z=&\frac{1}{\omega c_d}\frac{2}{\sigma^2+\omega^2\varepsilon_s^2}\left[\frac{\sigma(1-\cos\theta_2)+\omega\varepsilon_s\sin\theta_2}{\theta_1}\right]\\&-i\left\{\frac{1}{\omega c_d}-\frac{1}{\omega c_d}\frac{\zeta}{\sigma^2+\omega^2\varepsilon_s^2}\left[\frac{\sigma\sin\theta_2-\omega\varepsilon_s(1-\cos\theta_2)}{\theta_1}\right]\right\}\\&=R_d-ix_d\ \text{(ohm-cm}^2)\end{aligned} \tag{16}$$

Figure 5 shows the calculated small-signal impedances for a $p^+\nu np$ structure with $L=7.4\,\mu$m, $a_1=0.5\,\mu$m, $a_2=0.5\,\mu$m, $N_\nu=7\times10^{14}\,cm^{-3}$, $N_n=7\times10^1\,cm^{-3}$, and $N_A=1\times10^{14}\,cm^{-3}$. At 30 A/cm² the peak negative resistance $(-R_d)$ occurs at $f\simeq8.0$ GHz.

2. Large Signal Analysis

We shall use the same values of *dc* bias and frequency for our large signal analysis. Figure 6 shows the comparasion of the maximum negative resistance and the maximum operation efficiency as a function of *ac* signal amplitude for a p^+np^+ and $p^+\nu np$ diodes, their structure parameters are given in the Figure captions.

Figure 7 shows the frequency changes as the function of *dc* bias at maximum negative resistance and Figure 8 shows the output power and efficiency variations as a function of frequency. For an $M\nu np$ diode with the structure paraments as:

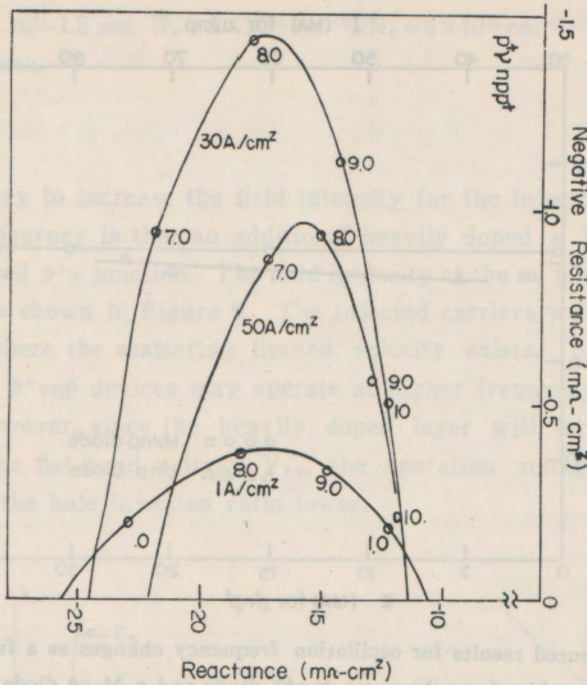

Fig. 5. Small-signal impedance for $p^+\nu np$ diode in the negative resistance region for three difference bias current. The device parameters are: $L=8.5$ cm, $a_1=0.5\ \mu$m, $a_2=1\ \mu$m, $N_\nu=7\times10^{14}$ cm^{-3}, $N_D=7\times10^{15}$ cm^{-3}, $N_A=7\times10^{14}$ cm^{-3}.

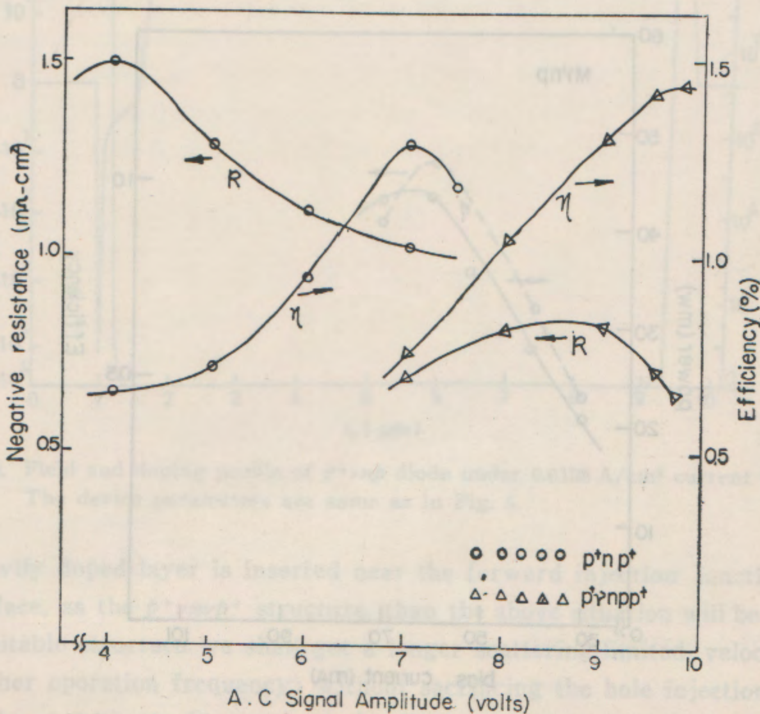

Fig. 6. Theoretical calculated results of maximum negative resistance and operation efficiency of the diodes of p^+np^+ and $p^+\nu np$ as the function of ac signal amplitude (The device parameters are same as what we mentioned).

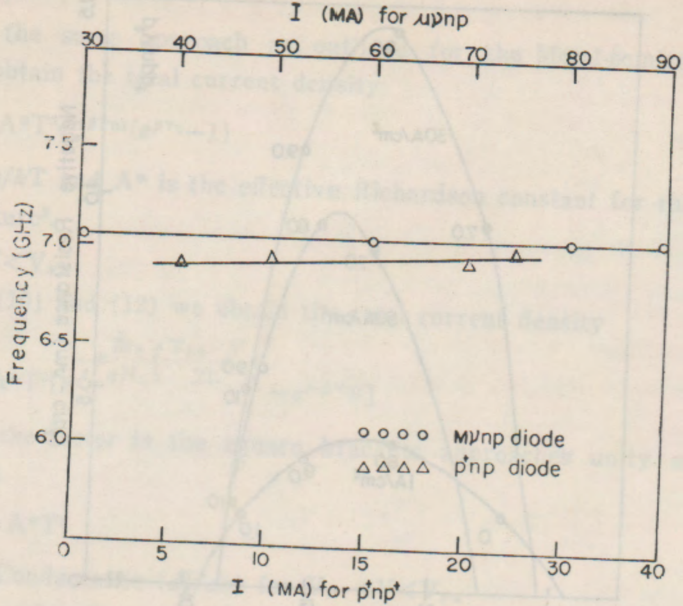

Fig. 7. Measured results for oscillation frequency changes as a function of *dc* current bias from the same p^+np^+ diode and a Mν*np* diode. The device parameters of the Mν*np* diode are: L=11 μm, a_1=1 μm, a_2=1.5 μm, N_ν = 2×10^{14} cm^{-3}, $N_D=5\times10^{15}$ cm^{-3}, $N_A=10^{14}$ cm^{-3}.

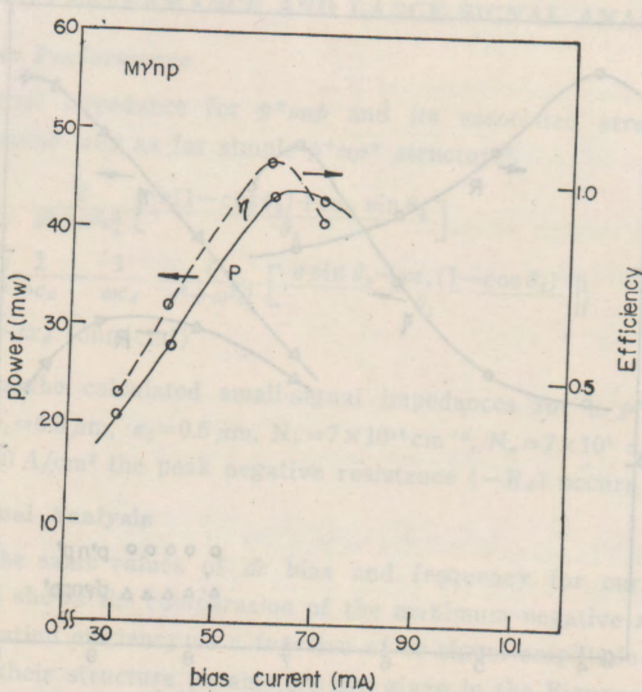

Fig. 8. The measured output power and efficiency as function of bias current for the Mν*np* diode (as described in Fig. 7). The area of the diode is 15 mil.

L=11 μm, a_1=1 μm, a_2=1.5 μm, $N_\nu=2\times10^{14}\ cm^{-3}$, $N_D=5\times10^{15}\ cm^{-3}$, $N_A=10^{14}\ cm^{-3}$ and with 15 mil diode area.

V. DISCUSSION

The simplest way to increase the field intensity for the injected carriers at the beginning of their journey is that an additional heavily doped *n* layer be inserted at the forward biased $p^+\nu$ junction. The field intensity at the $n\nu$ junction is increased, and much faster, as shown in Figure 9. The injected carriers will enter the drift region at a point where the scattering limited velocity exists. So that for a same physical length the $p^+\nu np$ devices may operate at higher frequency than the simply p^+np^+ devices. However, since the heavily doped layer will increase the built-in potential V_{D1} and the flat band voltage V_{FB}, the operation voltage is expected to increase and make the hole injection ratio lower.

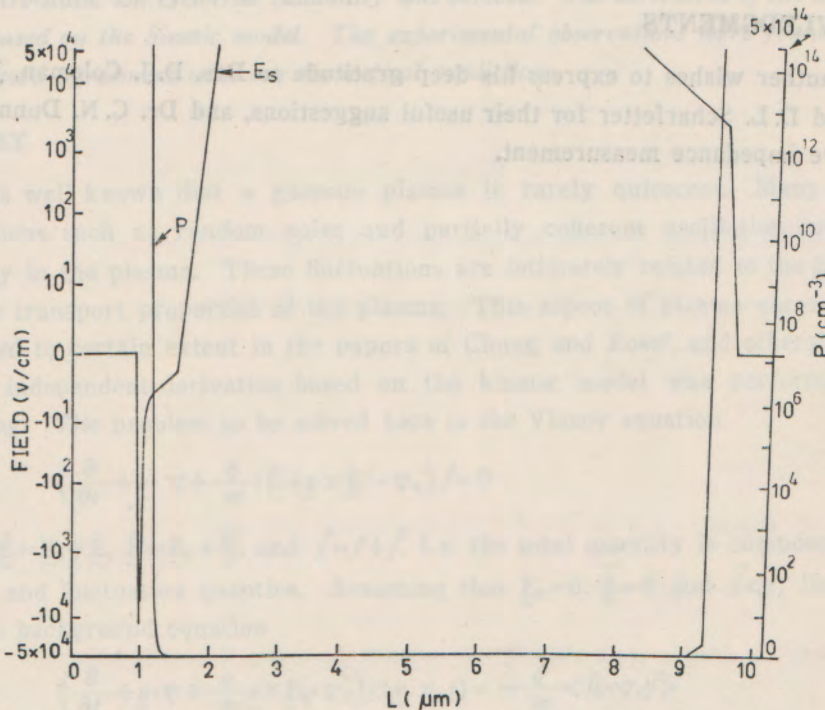

Fig. 9. Field and doping profile of $p^+\nu np$ diode under 0.0198 A/cm² current bias. The device parameters are same as in Fig. 5.

If a heavily doped layer is inserted near the forward injection junction instead at the interface, as the $p^+\nu n\nu p^+$ structure, than the above situation will be improved; i. e., with suitable structure we shall get a longer scattering-limited velocity region (also a higher operation frequency) without sacrificing the hole injection ratio and increasind the operating voltage too much. From the expression of V_{FB} we know that in order to maintain the lower operating voltage, we should make the width of the inserted *n* layer as narraw as possible.

In order to improve the structure further, we must adjust the electric field in the drift region, so that it is low but sufficient to maintain the carriers at their scattering-limited velocity. The requirement can be satisfied by the use of an ohmic pp^+ contact to replace the right side νp^+ contact. This in turn gives us the $p^+\nu np$ structure.

Another feature of the $p^+\nu np$ and its complementary structure is that the charge of the ionized impurities in the drift region are either heavily doped N_D^+ layer or N_A^- which has opposite polarity to that of the mobile carriers so that when the drift current density is comparable to ionized impurity density (i. e. $J \sim qV_sN_A$, where V_s is the scattering-limited velocity of the mobile carriers, and N_A the ionized impurity density in the p layer), the space charge limited effect can be reduced.

The field profile of $p^+\nu np$ structure under vary low bias current is shown in Figure 9. It shows the high field in the delay region, or drift region, also assure the possibility of obtaining a high *ac* field swing, and thus, high output power.

ACKNOWLEDGMENTS

The auther wishes to express his deep gratitude to Drs. D. J. Coleman, Jr. R. M. Ryder and D. L. Scharfetter for their useful suggestions, and Dr. C. N. Dunn for the microwave impedance measurement.